THE BELL SYSTEM TECHNICAL JOURNAL
Vol. 57, No. 1, January 1978
Printed in U.S.A.

Computer-Aided Magnetic Circuit Design for a Bell Ringer

By R. M. HUNT and J. W. NIPPERT

(Manuscript received June 17, 1977)

A general computer-aided design method for use with electromagnetic devices such as ringers, relays, and solenoids is described. The method is demonstrated by applying it to the design of polarized bell ringers. A lumped-element model with electrical, magnetic, and mechanical portions is used in the analysis. First, interaction equations are derived using a Lagrangian formulation applied to a simple model. Second, the model is refined by subdividing the iron members and including more leakage paths. An electrical circuit analysis program assembles the equations for the electromagnetic portion of this more complete model and produces a subroutine that solves these equations. A computer program has been written to predict the effects of changing motor parameters. The versatility and usefulness of the design technique has been demonstrated by applying it to the Bell System TRIMLINE® *telephone set ringer to achieve major design improvements.*

I. INTRODUCTION

In 1952 the Bell System introduced the standard 500-type telephone set which uses a "universal" two-gong ringer (C-type) to meet a wide variety of service conditions.[1] A universal ringer must: (*i*) have two voltage sensitivity modes that ensure adequate operation under worst-case conditions and provide protection against cross ringing on party lines, (*ii*) be electrically polarized to protect against bell tapping due to dialing transients, (*iii*) have high impedance (≈8 kohms) at ringing voltages so that multiple ringers can be bridged across the line, (*iv*) have high impedance (≈120 kohms) at voice frequencies to prevent speech signal attenuation, and (*v*) have two coil windings for use with multiparty ringing circuits.[2]

Recently a project was undertaken to design a miniature single-gong ringer that would have the low cost, reliability, sensitivity, and sound

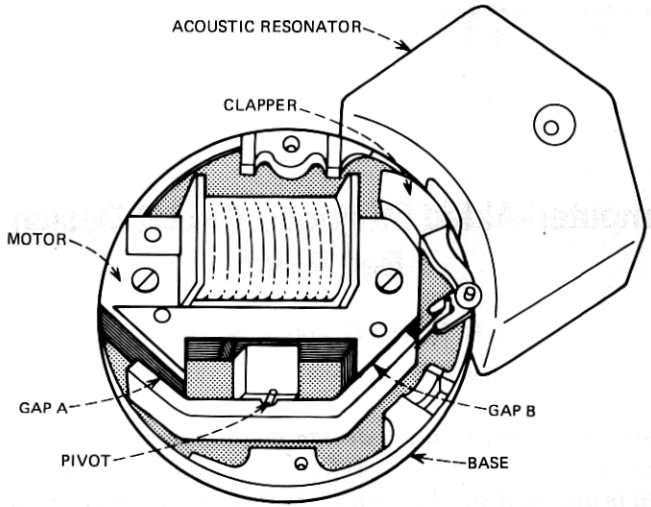

Fig. 1—Ringer with rocking-armature motor (gong and clamp plate removed).

output of the C-type ringer but would be significantly smaller. The small single-gong P-type ringer commonly used in *TRIMLINE*® telephones and other new telephone sets did not optimally meet all of these objectives and previous attempts to meet them were unsuccessful. To achieve these objectives, effort was channeled toward a rocking armature type motor[3,4] that drives a single clapper and fits under the gong. A mathematical model was essential for the design process in order to perform parametric analyses and design optimization. The mathematical model had to realistically account for flux saturation of materials and flux leakage paths in the design, both of which have significant influence on the performance of a compact ringer motor.

II. RINGER OPERATION

The structure of a ringer with a rocking armature motor is shown in Fig. 1 and an exploded view of the motor is shown in Fig. 2. In the absence of coil current a bias spring (not shown) returns the armature to the position shown in Fig. 1. The permanent magnet flux passes through both armature gaps and nearly saturates the shunt member. The ringer is electrically polarized since only coil current of one polarity will cause operation. Coil current in the operate direction increases the flux in gap A and decreases the flux in gap B causing clockwise armature rotation which drives the clapper away from the gong. As the current returns to zero the armature returns to its normal position and drives the clapper into the gong. For negative coil current the shunt member of the magnetic circuit has a relatively low reluctance so that most of the coil flux

passes through the shunt instead of the working gaps. The low reluctance shunt results in the ringer having a high electrical inductance which is necessary for resonance of the ringer circuit at the frequency of the ringing power supply, 20 Hz.

The ringer motor consists of a bobbin-wound coil, a pole piece assembly, a permanent magnet, a pivot pin, and an armature of low carbon steel. Figure 2 shows one version of the rocking armature motor which

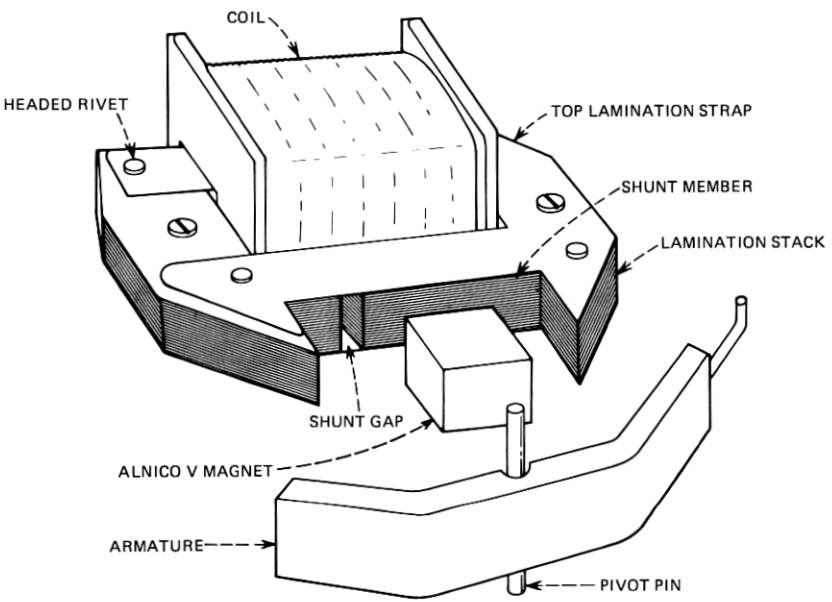

Fig. 2—Rocking-armature motor.

is described in this paper. In this version the pole piece assembly consists of two lamination stacks sandwiched between two silicon steel lamination straps and held together with three aluminum rivets.

Basic motor performance is usually studied using measured static torque curves that show the relationship between blocked armature torque, armature position, and dc coil current. Figure 3 shows two idealized torque curves, one with the armature blocked in the nonoperate position (gap B closed) and the other with the armature blocked in the operate position (gap A closed). A single cycle of very slowly varying coil current is shown below the torque curves to illustrate the quasistatic operation of the motor. A major objective of the mathematical model described here was the prediction of static torque curves from basic motor parameters such as dimensions, material magnetic characteristics, and armature displacement.

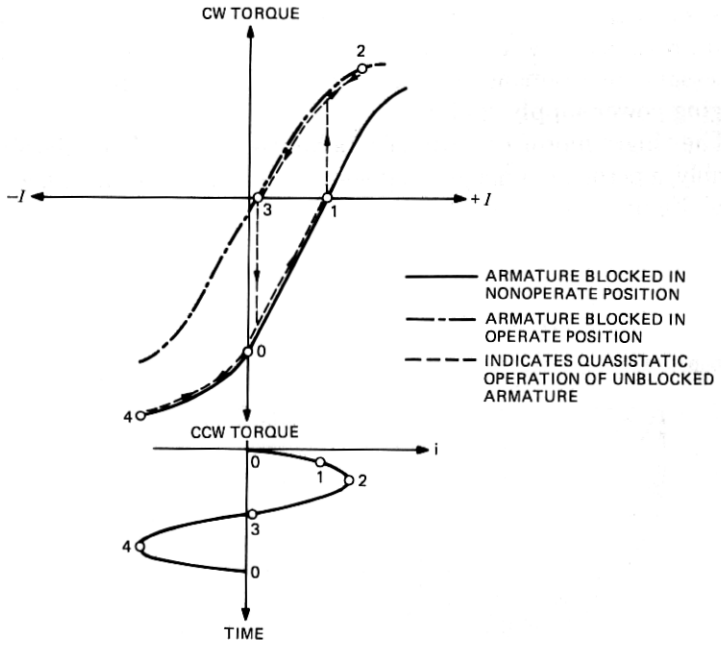

Fig. 3.—Ringer motor static torque curves and quasistatic operation.

III. MATHEMATICAL MODEL

Successful methods of modeling electromechanical devices such as relays and solenoids have appeared elsewhere.[5,6] The electromechanical ringer is a complex device and a complete analysis would involve the solution of Maxwell's three-dimensional field equations in space occupied in part by nonlinear material with memory. Fortunately, because ringers are low-frequency and low-velocity devices, the following simplications can be made for design analysis:

(*i*) The field problem can be approximated by a network where each volume of space occupied by a uniform material is represented as one or more lumped elements. Each element represents a physical effect in the uniform member, such as reluctance or loss.

(*ii*) All magnetic members except the permanent magnet are assumed not to have memory (no hysteresis).

(*iii*) Stray flux paths through air can be adequately represented by lumped leakage reluctances.

A lumped-element model for the magnetic portion of the motor of Fig. 2 appears in Fig. 4. This model uses the common flux-current analogy between magnetic circuits and electric circuits. Iron members are modeled by nonlinear reluctances and are characterized by normal *B-H*

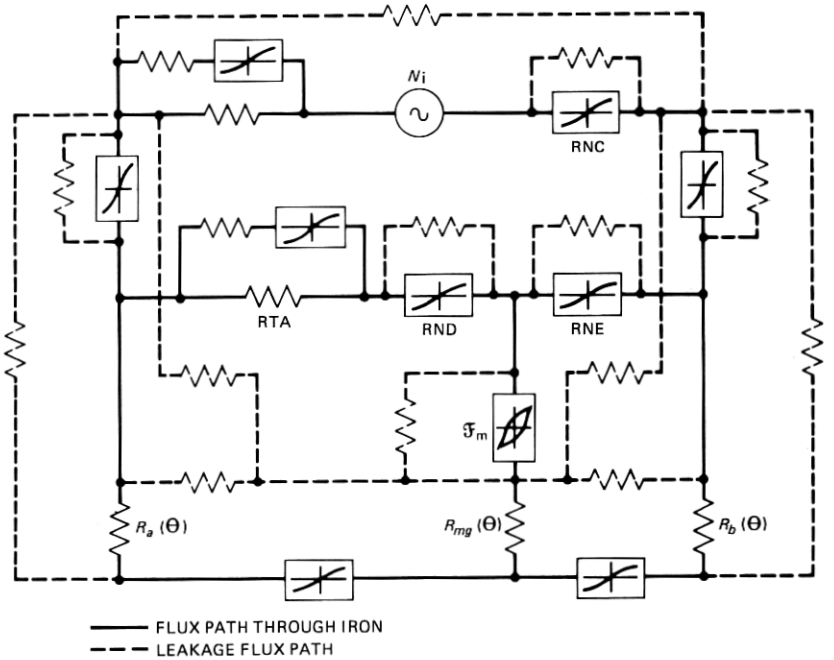

Fig. 4—Lumped element model (equivalent circuit) for magnetic portion of rocking-armature motor.

curves. The magnet is modeled using its demagnetization (de-mag) curve and recoil permeability. A function was fitted to reference data for the *B-H* characteristics. The fitting process and results are described in Appendix A.

Leakage flux paths are modeled by lumped reluctances. The number and magnitude of these reluctances were determined from available formulae and prototype measurements as described in Appendix B.

IV. EQUATION FORMULATION

A consistent way to develop the equations for a system that has mechanical, magnetic, and electrical energy is to use the Lagrangian formulation. The procedure is illustrated in Appendix C by applying it to the simplified model of Fig. 5. The equilibrium equations for the simplified model are a set of five differential equations, one electrical, one mechanical, and three magnetic, the simultaneous solution of which describes the dynamic performance of the motor.

The equilibrium equations are reduced to the static case since only quasistatic motor performance is considered here. In the resulting set of nonlinear equations the current source becomes a magnetomotive source *NI* in one of the magnetic equations and the mechanical equation

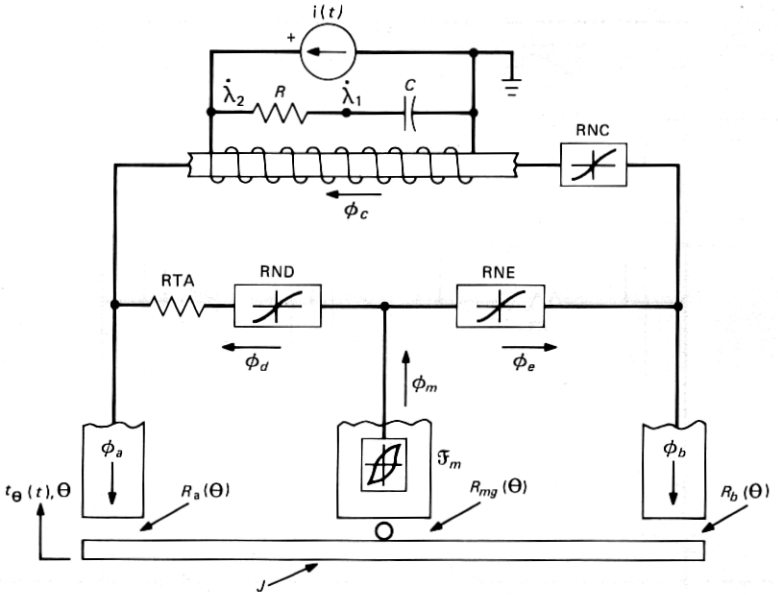

$\dot{\lambda}_1$ = VOLTAGE ACROSS CAPACITOR
$\dot{\lambda}_2 = N\dot{\phi}_c$ = VOLTAGE ACROSS COIL
J = ARMATURE MOMENT OF INERTIA
$t_\Theta(t)$ = EXTERNALLY APPLIED TORQUE
$\mathfrak{F}_m$ = MAGNET MAGNETOMOTIVE FORCE
ϕ = MAGNETIC CIRCUIT FLUX

Fig. 5—Simplified lumped element model for rocking-armature motor.

gives the static torque on the armature. See Appendix C, eq. (21). Armature torque t_o is given by

$$t_o = -\frac{\phi_a^2}{2P_a^2}\frac{\partial P_a}{\partial \theta} - \frac{\phi_b^2}{2P_b^2}\frac{\partial P_b}{\partial \theta} - \frac{(\phi_a + \phi_b)^2}{2P_{mg}^2}\frac{\partial P_{mg}}{\partial \theta}$$

where the ϕ's and P's are the gap fluxes and permeances respectively. Magnetic permeance is the reciprocal of reluctance.

It is apparent from this equation that for accurate calculations of torque, appropriate functions for gap permeance must be determined. This is done in Appendix D. The gap fluxes are found by solving the three magnetic equations for specified values of coil current and armature displacement. The gap fluxes are then used in the torque equation above. To achieve accurate calculations of circuit fluxes it was found necessary to include up to 30 elements in the magnetic portion of the model.

Having used the Lagrangian formulation to determine the terms of mechanical-magnetic interaction for the simplified model, circuit

analysis techniques were then used to generate the equations for the electromagnetic portion of the more complex model shown in Fig. 4. This step permitted increasing model complexity to account for significant measured effects without tedious derivation of new equilibrium equations.

V. SOLUTION OF EQUATIONS

The next task is to find the solution to a set of simultaneous nonlinear equations. Since linear equations are easy to solve, at least in principle, the set of nonlinear equations may be solved most easily by finding a sequence of solutions to related linear equations that converges to the solution of the nonlinear equations. In general, closed-form (exact) solutions do not exist for nonlinear systems, so some such iterative method of solution must be used.

The procedure adopted is well known as Newton's method. The nonlinear system is expanded in a Taylor series about some trial solution. Retaining only the linear terms in this expansion, the resulting set of linearized equations is solved to yield a new approximation to the solution. Successive solutions converge to the solution of the original nonlinear system.

The magnetic portion of the more complex model was analyzed using the Circuit Analysis Program for Efficient Computer Optimized Design (CAPE COD).[7] From a topological input description of the magnetic circuit, CAPE COD produces a subroutine that solves the network equations. This routine is combined with the interaction terms derived from the Lagrangian formulation to provide the complete device model for the static case.

5.1 Sequence of analyses

The first calculation procedure determines a maximum operating point for the magnet. For this calculation, the magnet is described by its de-mag B-H curve, and the independent coil current source is set to zero. A tentative operating point is found by iteration, as described above. Once this maximum operating point is determined, the operating point of the magnet is lowered until the ringer will just begin to operate at a specified current. The results of this analysis are then printed.

A graph for the de-mag B-H curve for the magnet and the "load line" of the rest of the circuit as seen by the magnet is produced. For this calculation of the load line, a value for H is selected, and the slope of the B-H curve for the magnet is set to zero. The solution of this system gives the corresponding value of B on the load line for the selected H. The independent source associated with the coil is again set to zero for these calculations.

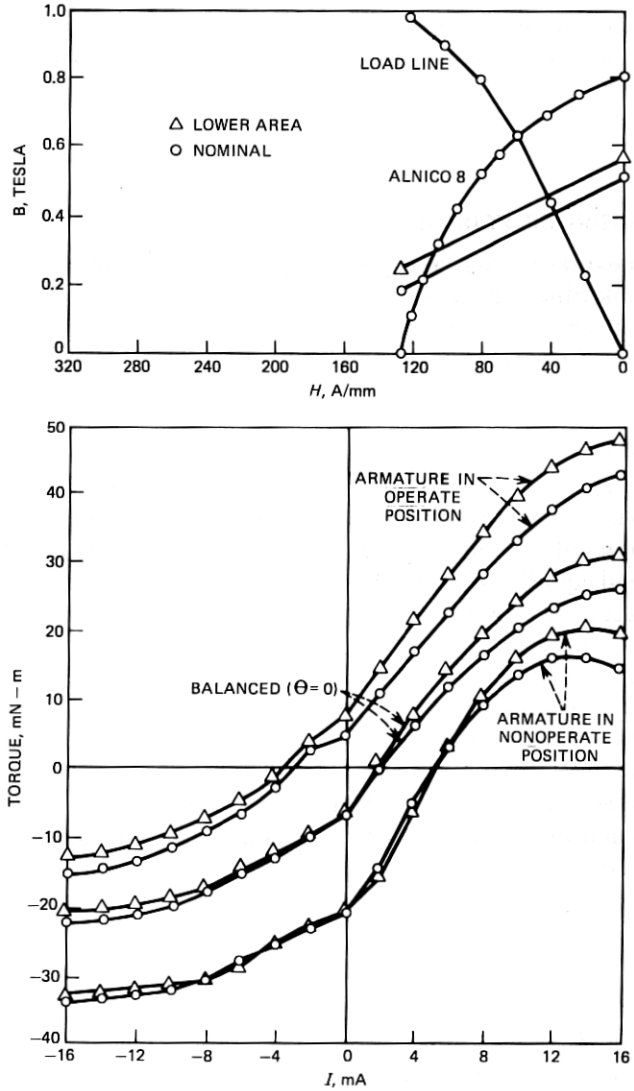

Fig. 6—Typical program output showing the predicted effect of decreasing the cross-sectional area of a magnetic shunt member.

To calculate torques, the magnet characteristic used is that of the recoil line through the final operating point. The independent source associated with the coil is set to the appropriate ampere-turns, and the calculations proceed as before. The torque on the armature is calculated from the flux through the gaps at the armature. The displacement of the armature and the ampere-turns of the source are varied to produce a family of curves. Figure 6 is a sample of the plotted program output

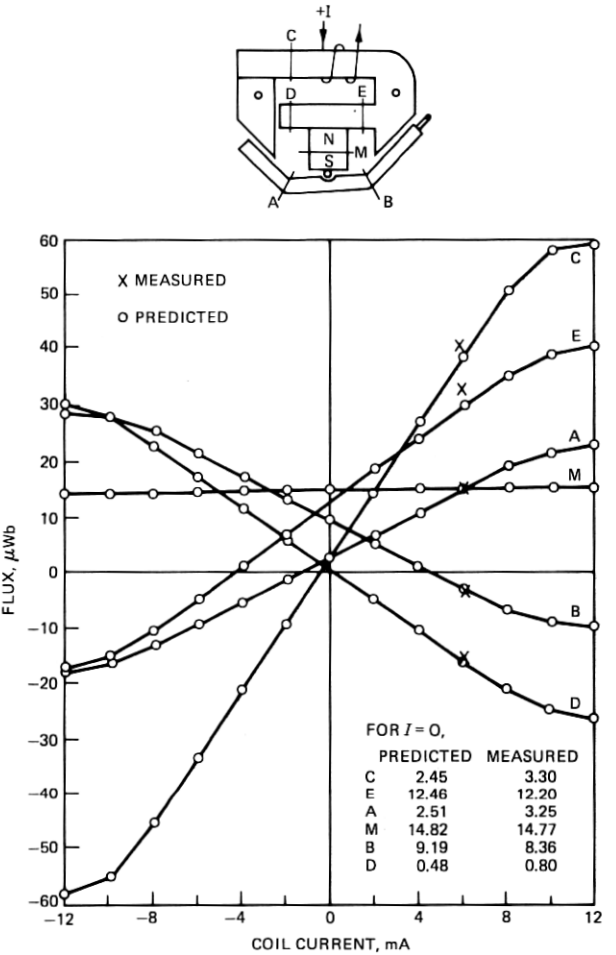

Fig. 7—Flux versus coil current, predicted and measured.

showing both the permanent magnet and torque characteristics of a motor and the predicted effect of changing a single parameter, the cross-sectional area of the shunt.

VI. VERIFICATION OF MATHEMATICAL MODEL

Measurements were made on an early prototype of the rocking armature motor in order to verify the mathematical model. The solid curves of Fig. 7 show the predicted flux versus coil current in key magnetic members. Measured fluxes, some of which are indicated, showed good agreement with predicted values. Agreement was particularly good for fluxes ϕ_a and ϕ_b, which determine armature torque.

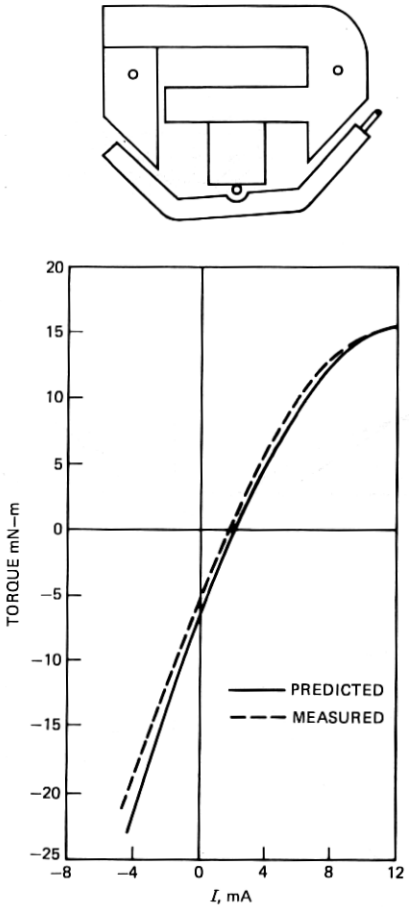

Fig. 8—Predicted and measured torque curves.

The comparison of predicted to measured armature torque is shown in Fig. 8. Agreement between these two curves is very satisfactory. A comparison of the predicted to measured effect of changing two important variables, armature displacement and magnet strength, is shown in Fig. 9. The measured change is considered to show adequate agreement, especially in the important midrange currents where ringer bias adjustments are made.

VII. OPTIMIZATION

The mathematical model of the ringer motor aided first in identifying key parameters and second in finding a set of parameter values which optimize motor performance. The General Purpose Optimization Package (GPOP)[7] was combined with the ringer analysis program to

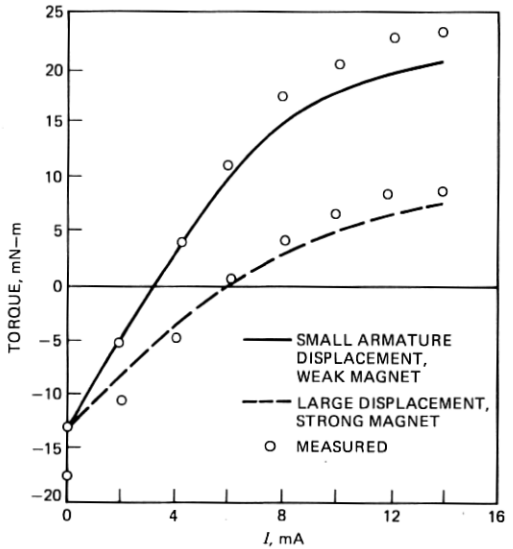

Fig. 9—Predicted and measured effects of parameter changes.

perform that optimization. First a criterion function based on the desired motor characteristics was developed. Second, the program determined a set of values for the parameters that improves the performance of the ringer relative to a set of initial values provided to the program.

7.1 Desired motor output

Basic motor performance is evaluated through use of static torque curves. The two idealized torque curves of Fig. 3 are shown in Fig. 10, with important points indicated. The two "stick" torques are defined to occur at zero current with the armature on either pole. They are indicated on the figure by the labels T_a and T_b. Torque T_a must be either negative (counterclockwise) or, if positive (clockwise), must be small enough to be overcome by a practical bias spring. This ensures that the armature always returns to its nonoperate position in the absence of coil current.

Torque T_b must be large enough to drive the clapper against the gong with sufficient velocity. At the same time T_b must not be so large that excessive armature impact noise and wear are produced by the armature striking pole B.

Of primary importance is the slope of the nonoperated torque curve immediately above turn-on current I_1. This is called the motor torque factor and should be as high as possible to facilitate ringer sensitivity adjustments and to maximize ringer reliability. The slope between I_2 and I_3 is usually lower than that between I_1 and I_2 but must be high

enough to prevent reliability problems in high ringing-voltage situations with the ringer bias spring in its high-tension position.

Another important criterion is the inductance of the ringer. The change in flux through the coil between peak currents was taken as an approximation to the inductance.

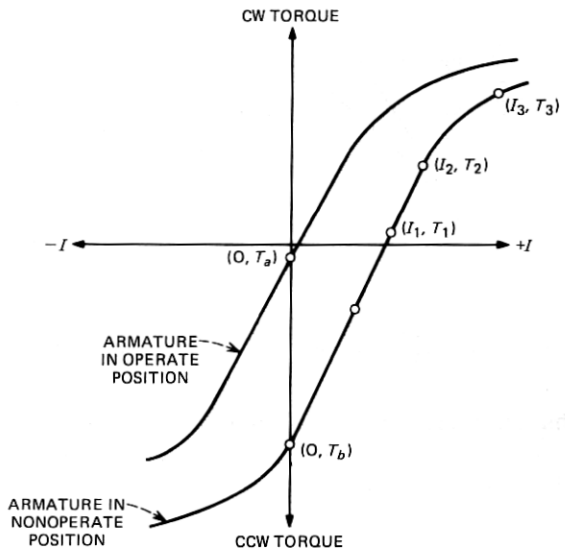

Fig. 10—Idealized torque curves.

7.2 Criterion function

From these diverse requirements a function is formed that expresses in a single number a measure of performance for a ringer built to match any given set of parameters. The form of the function selected involves the use of penalty functions. The idea is fairly simple. To a function describing how good the performance is, functions are added that are zero if a given constraint is satisfied and nonzero if the constraint is violated. Appendix E shows the function used.

VIII. RESULTS

8.1 Rocking armature motor

The modeling technique was used to evaluate variations of the basic rocking armature motor so as to best meet the diverse requirements. Based on the theoretical results obtained, laboratory models of ringer

designs were built and evaluated in terms of the Bell System ringer requirements. Figure 11 shows a motor design which meets requirements and appears simple to manufacture. Iron straps are used to sandwich the lamination stacks and also to reduce flux densities in the assembly. A short Alnico 8 magnet is used which allows the use of a straight armature. Figure 12 shows the predicted and measured results of an optimization run. As shown, a significant reduction in pole A stick torque

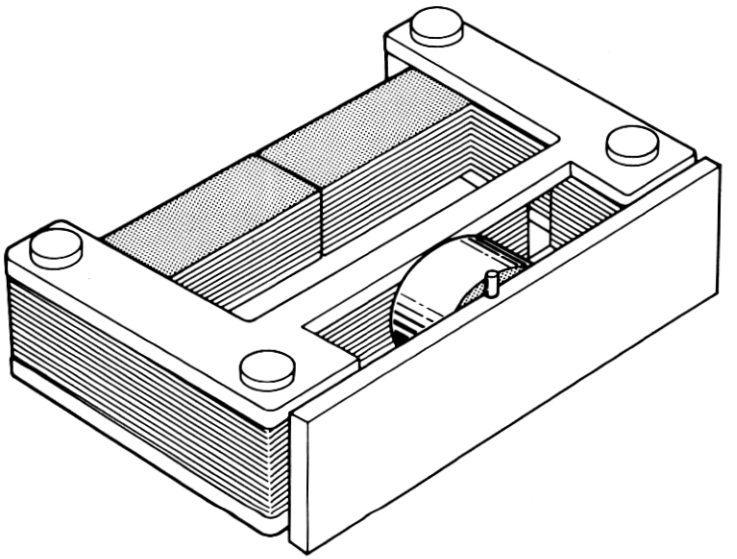

Fig. 11—Ringer motor with straight armature.

is achieved, but with a sacrifice in torque factor. Further evaluation and refinement of this rocking armature design was not pursued since effort was turned toward improving the P-type ringer as described below.

8.2 Bell System P-type ringer

The analysis techniques developed for the rocking armature motor were applied to the Bell System small P-type ringer. The objective was to investigate potential improvements to the torque curve with simple design changes. Figure 13 shows the motor structure which is a single-ended rocking-armature type with air gaps on opposite sides of the armature. Figure 14 shows the equivalent circuit used to analyze it. It was predicted and then verified with measurements that a significant improvement in torque factor is achieved with two basic design changes. First, the magnetic bias force is reduced by moving the pivot pin closer to the magnet center. This results in higher magnet flux after the mag-

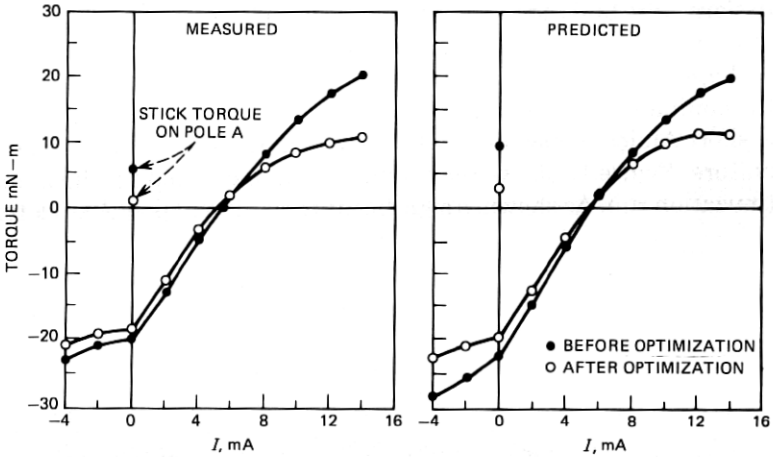

Fig. 12—Predicted and measured effect of optimized parameters.

netization adjustment. Secondly, the flux density at a critical point of saturation is reduced by increasing the cross-sectional area of the pole piece. The measured results are shown in Figure 15.

IV. CONCLUSIONS

A general method of computer-aided design for electromagnetic devices has been presented. The method was applied to the design of two polarized bell ringer motors. A mathematical model and computer simulation of the rocking armature motor made it possible to accurately and efficiently study motor performance as a function of the many parameters involved. The simulation methods were also applied to the P-type ringer commonly used in the *TRIMLINE* telephone and resulted

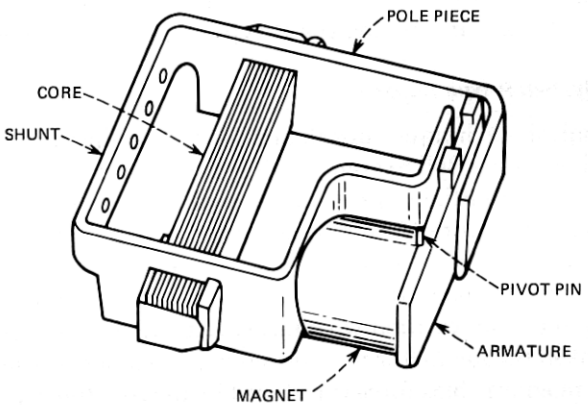

Fig. 13—P-type ringer motor.

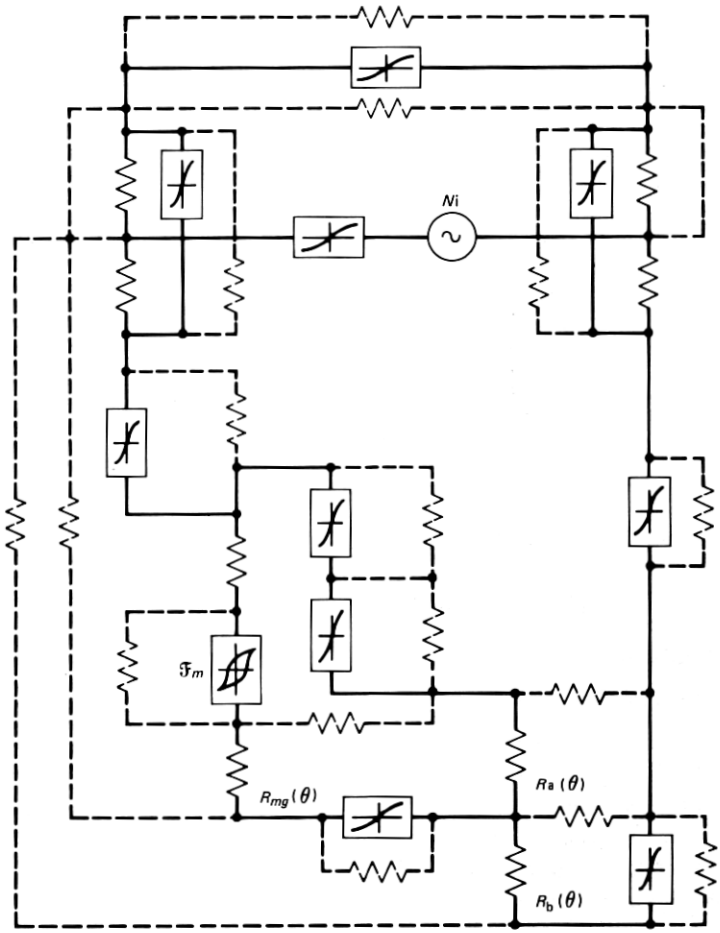

Fig. 14—Lumped element model of P-ringer motor.

in a significantly higher torque factor. This improvement in addition to others not covered here have led to a modified P ringer virtually meeting the original goals of the rocking armature ringer development.

X. ACKNOWLEDGMENTS

The authors are indebted to P. O. Schuh for suggesting the Lagrangian formulation. D. P. Borenstein, G. M. C. Fisher, D. J. Leonard, E. A. Mills, M. L. Warnock, R. S. Weiner, and K. B. Woodard supported and encouraged the effort. L. A. Marcus, N. B. Karu, and W. F. Wernet aided in the physical design and dynamic measurements of later models.

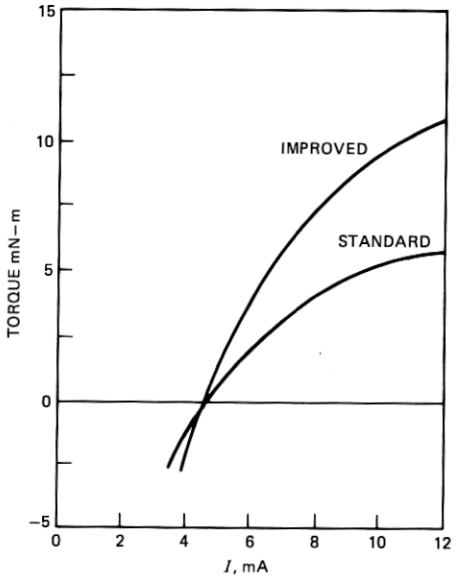

Fig. 15—P-type ringer motor measured torque curves.

APPENDIX A

Iron member characterization

The characteristics of an iron member are modeled using the element's length, width, and the normal B-H curve for the material. Several methods have been used for representing this curve: a table of (B,H) pairs may be given, simple hyperbolas may be fit to a range of the curve, a series of exponentials may be fit to the curve, a function of a polynomial divided by another polynomial (rational function) may be fit to the data. For this analysis H is given as the ratio of two polynomials in B.

A family of functions with numerator and denominator polynomials of varying orders was fitted to the data. The function selected from this family provided a good combination of low order, close approximation to the data being fitted, and smooth behavior of the derivative. Figure 16 shows the selected curve fit and the data points used in the fitting process.

APPENDIX B

Leakage elements

Leakage elements are reluctances which represent stray flux paths through air from two points in the magnetic circuit. Leakage elements placed across nonlinear magnetic elements reduce the sharpness with which the elements go into saturation and are essential to obtaining agreement between predicted and measured fluxes.

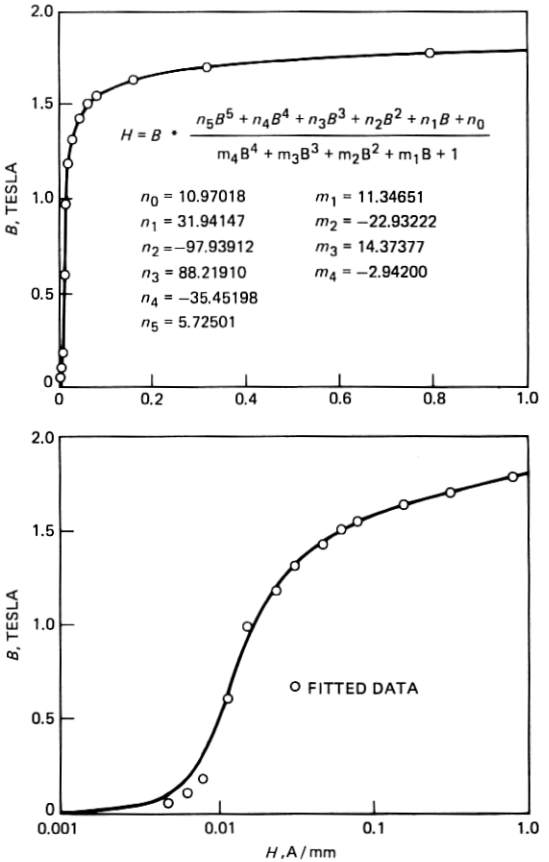

Fig. 16—*BH* curve fit for silicon steel.

The number of leakage elements and their placement in the model can be observed by sprinkling iron fillings on a prototype as shown in Fig. 17. Precise numerical values of these leakage elements are difficult to obtain. However, the method of "estimating the permeances of probable flux paths" from Ref. 8 has proven useful in obtaining first-order estimates. Also, low-frequency inductance measurements of partial motor assemblies can be used to estimate leakage around the coil. Flux measurements on the physical model are then used to refine the initial estimates. Once determined, the leakage reluctances remain constant unless major changes in geometry are made.

APPENDIX C

Lagrangian formulation

The first step for the Lagrangian formulation is to select an appropriate set of generalized coordinates which define the state of the system.

Typically these are flux linkage, node voltage, capacitor charge, inductor currents, and physical displacements. For this ringer analysis, coordinates representing linkage, node voltage, and angular displacement of the armature where selected.

The second step of the procedure requires formulation of the Lagrangian function and a Rayleigh dissipation function in terms of the generalized coordinates. Since most power dissipation occurs in winding resistance and since the technique becomes burdensome with individual hysteresis and eddy current loss elements, a single electrical loss element was assumed to account for the total system dissipation.

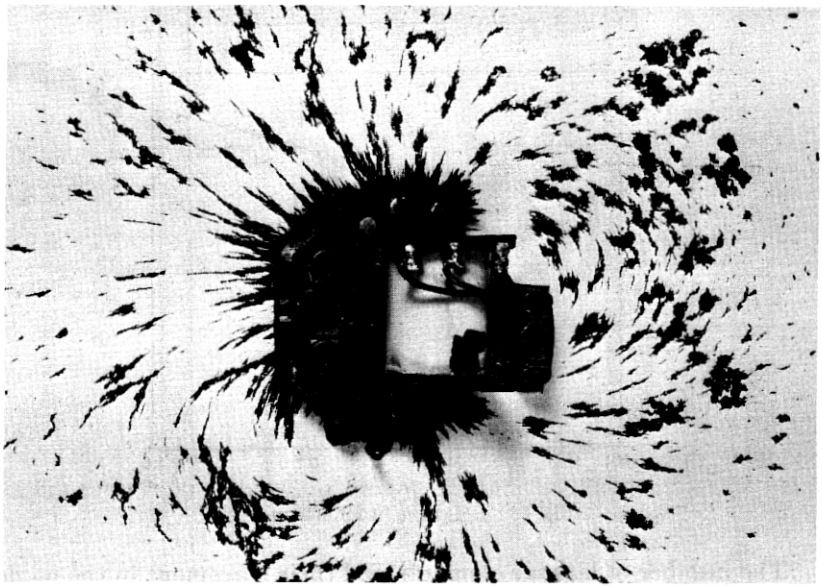

Fig. 17—Prototype ringer with iron filings.

The third step applies Lagrange's formula to the energy functions to produce a set of simultaneous differential equations. Primarily this involves taking partial derivatives and collecting terms.

The advantage of this technique is that it systematically accounts for the interaction between the magnetic and mechanical portions of the system. The disadvantages are as follows: first, the choice of generalized coordinates is not necessarily obvious; second, hysteresis and other losses are difficult to fit into the formulation.

The Lagrangian $\mathcal{L}$ is defined as the difference between the total system coenergy function $\mathcal{T}'$ and the total system energy function $\mathcal{V}$ as defined below. Choosing a nodal formulation for the electrical portion

of the system and using the functional dependencies prescribed in Ref. 9 we have:

$$\mathcal{L}(\dot{\theta},\theta,\dot{\lambda},\lambda,t) = \mathcal{T}'(\dot{\theta},\theta,\dot{\lambda},t) - \mathcal{V}(\theta,\lambda,t) \tag{1}$$

where θ is the angular displacement of the armature, λ is the flux linkage, t is time and dots above quantities denote differentiation with respect to time.

The system coenergy function is the sum of the mechanical (kinetic) and electrical coenergy functions:

$$\mathcal{T}'(\dot{\theta},\theta,\dot{\lambda},t) = T'(\dot{\theta},\theta,t) + W'_e(\dot{\lambda},\theta) \tag{2}$$

The system energy function is the sum of mechanical (potential) and magnetic energy functions:

$$\mathcal{V}(\theta,\lambda,t) = V(\theta,t) + W_m(\lambda,\theta) \tag{3}$$

For the system of Fig. 5 the mechanical coenergy function is

$$T'(\dot{\theta},t) = \frac{1}{2}J\dot{\theta}^2 \tag{4}$$

where J is the moment of inertia of the armature about the pivot axis. The electrical coenergy function is:

$$W'_e(\dot{\lambda}_1) = \frac{1}{2}C\dot{\lambda}_1^2 \tag{5}$$

where C is the value of the ringing capacitor. The total system coenergy function now becomes:

$$\mathcal{T}'(\dot{\theta},\lambda_1,t) = \frac{1}{2}J\dot{\theta}^2 + \frac{1}{2}C\dot{\lambda}_1^2 \tag{6}$$

Since no change in mechanical potential energy is assumed, it remains to find the magnetic energy function, W_m. The energy W in a lumped magnetic element of length ℓ, area A, flux density B and magnetic field H can be approximated by the following integral:

$$W = \ell A \int_o^B H(B')\,dB' \tag{7}$$

Since $B = \phi/A$,

$$W = \int_o^{\phi} \ell H\left(\frac{\phi'}{A}\right) d\phi' = \int_o^{\phi} \mathcal{F}\left(\frac{\phi'}{A}\right) d\phi', \tag{8}$$

where ℓH is called the magnetomotive force (MMF) and is labeled $\mathcal{F}$.

For linear magnetic elements $\mathcal{F}$ is a linear function of flux, i.e., $\mathcal{F} = R\phi$, where R is the reluctance of the element and defined as $\ell/\mu_o A$.

Therefore the energy in a linear element is:

$$W = \int_o^{\phi} R\phi' \, d\phi' = \frac{1}{2} R\phi^2. \tag{9}$$

In a system model that includes more magnetic elements than those which directly link the coil, it is convenient to use flux (ϕ) for coordinates in the magnetic portion of the circuit rather than flux linkage (λ). Both have the same dimensions, differing only by the dimensionless quantity, number of turns.

The total magnetic energy function, W_m, can now be expressed by summing the energy of magnetic elements:

$$\begin{aligned} W_m(\phi_i,\theta) = {} & \frac{1}{2} R_a(\theta)\phi_a^2 + \frac{1}{2} R_b(\theta)\phi_b^2 + \frac{1}{2} R_{mg}(\theta)\phi_m^2 \\ & + \frac{1}{2} R_{ta}\phi_d^2 + \int_o^{\phi_m} \mathcal{F}_m(\phi'_m)\, d\phi'_m + \int_o^{\phi_d} \mathcal{F}_d(\phi'_d)\, d\phi'_d \\ & + \int_o^{\phi_e} \mathcal{F}_e(\phi'_e)\, d\phi'_e + \int_o^{\phi_c} \mathcal{F}_c(\phi'_e)\, d\phi'_e \end{aligned} \tag{10}$$

Note that the first three terms are gap energies and are functions of armature displacement. The last four terms are the energies in the nonlinear elements.

Continuity of flux in the magnetic circuit provides the following constraint equations:

$$\begin{aligned} \phi_m &= \phi_a + \phi_b \\ \phi_d &= \phi_a - \phi_c \\ \phi_e &= \phi_c + \phi_b \end{aligned} \tag{11}$$

After substituting the constraint equations into eq. (10) and then using eqs. (3), (6), and (10) in (1), the Lagrangian becomes:

$$\begin{aligned} \mathcal{L}(\dot\theta,\theta,\dot\lambda_1,\phi_i,t) = {} & \frac{1}{2} J\dot\theta^2 + \frac{1}{2} C\dot\lambda_1^2 - \frac{1}{2} R_a(\theta)\phi_a^2 \\ & - \frac{1}{2} R_b(\theta)\phi_b^2 - \frac{1}{2} R_{mg}(\theta)(\phi_a + \phi_b)^2 - \frac{1}{2} R_{ta}(\phi_a - \phi_c)^2 \\ & - \int_o^{\phi_a+\phi_b} \mathcal{F}_m(\phi'_m)\, d\phi'_m - \int_o^{\phi_a-\phi_c} \mathcal{F}_d(\phi'_d)\, d\phi'_d \\ & - \int_o^{\phi_c+\phi_b} \mathcal{F}_e(\phi'_e)\, d\phi'_e - \int_o^{\phi_c} \mathcal{F}_c(\phi'_c)\, d\phi'_c \end{aligned} \tag{12}$$

The Rayleigh dissipation function D is

$$D = \int_o^{\dot\lambda_r} \frac{\dot\lambda'_r}{R}\, d\dot\lambda'_r = \frac{\dot\lambda_r^2}{2R} = \frac{(\dot\lambda_2 - \dot\lambda_1)^2}{2R} = \frac{(N\dot\phi_c - \dot\lambda_1)^2}{2R} \tag{13}$$

where $\dot{\lambda}_r$ is the voltage across resistor R and the voltage across the coil $\dot{\lambda}_2$ is equal to $N\dot{\phi}_c$.

Lagrange's formula can now be applied:

$$\frac{d}{dt}\left(\frac{\partial \mathcal{L}}{\partial \dot{q}_i}\right) - \frac{\partial \mathcal{L}}{\partial q_i} + \frac{\partial D}{\partial \dot{q}_i} = Q_i \tag{14}$$

For the electrical coordinate λ_1, we have

$$C\ddot{\lambda}_1 - \frac{1}{R}(N\dot{\phi}_c - \lambda_1) = 0 \tag{15}$$

For the mechanical coordinate θ we have

$$J\ddot{\theta} + \frac{\phi_a^2}{2}\frac{\partial R_a}{\partial \theta} + \frac{\phi_b^2}{2}\frac{\partial R_b}{\partial \theta} + \frac{(\phi_a + \phi_b)^2}{2}\frac{\partial R_{mg}}{\partial \theta} = t_\theta(t) \tag{16}$$

For the magnetic coordinates ϕ_a, ϕ_b, and ϕ_c we have

$$\begin{aligned}
&(R_a + R_{mg} + R_{ta})\phi_a + R_{mg}\phi_b - R_{ta}\phi_c \\
&\qquad + \mathcal{F}_m(\phi_a + \phi_b) + \mathcal{F}_d(\phi_a - \phi_c) = 0 \\
&R_{mg}\phi_a + (R_b + R_{mg})\phi_b + \mathcal{F}_m(\phi_a + \phi_b) \\
&\qquad + \mathcal{F}_e(\phi_c + \phi_b) = 0 \\
&\mathcal{F}_c(\phi_c) + \mathcal{F}_e(\phi_c + \phi_b) + \mathcal{F}_d(\phi_a - \phi_c) - R_{ta}\phi_a + R_{ta}\phi_c \\
&\qquad + \frac{N}{R}(N\dot{\phi}_c - \dot{\lambda}_1) = Ni(t)
\end{aligned} \tag{17}$$

where R_a, R_{mg}, and R_b are understood to be functions of θ. After the permanent magnet has been charged and then stabilized, its second quadrant minor loop operation is modeled by a source of constant magnetomotive force, $-F_s$, in series with an internal magnet reluctance R_m. Thus,

$$\mathcal{F}_m(\phi_a + \phi_b) = -F_s + R_m(\phi_a + \phi_b) \tag{18}$$

The five equilibrium equations are then reduced to the static case by setting all time derivatives to zero and representing constant coil current and armature torque by I and t_o respectively:

$$\begin{aligned}
&(R_a + R_{mg} + R_{ta} + R_m)\phi_a + (R_{mg} + R_m)\phi_b \\
&\qquad - R_{ta}\phi_c + \mathcal{F}_d(\phi_a - \phi_c) = F_s \\
&(R_{mg} + R_m)\phi_a + (R_b + R_{mg} + R_m)\phi_b + \mathcal{F}_e(\phi_c + \phi_b) = F_s \\
&-R_{ta}\phi_a + R_{ta}\phi_c + \mathcal{F}_c(\phi_c) + \mathcal{F}_e(\phi_c + \phi_b) - \mathcal{F}_d(\phi_a - \phi_c) = NI
\end{aligned} \tag{19}$$

$$\frac{\phi_a^2}{2}\frac{\partial R_a}{\partial \theta} + \frac{\phi_b^2}{2}\frac{\partial R_b}{\partial \theta} + \frac{(\phi_a + \phi_b)^2}{2}\frac{\partial R_{mg}}{\partial \theta} = t_o \tag{20}$$

The result is three nonlinear algebraic magnetic equations (19) which must be solved for the three unknown fluxes. Fluxes ϕ_a and ϕ_b are then used in the mechanical eq. (20) for calculating torque developed on the armature. For convenience in handling gap functions, the torque equation is rewritten in terms of gap permeances (reciprocal of reluctance):

$$-\frac{\phi_a^2}{2P_a^2}\frac{\partial P_a}{\partial \theta} - \frac{\phi_b^2}{2P_b^2}\frac{\partial P_b}{\partial \theta} - \frac{(\phi_a + \phi_b)^2}{2P_{mg}^2}\frac{\partial P_{mg}}{\partial \theta} = t_o \tag{21}$$

APPENDIX D

Working gap functions

Since armature torque is determined from gap permeances and the partial derivatives of these permeances with respect to armature displacement, accurate mathematical expressions (gap functions) for these permeances must be derived. Gap functions which account for both fringing flux and main gap flux between nonparallel surfaces can be derived by use of the principles given by Roters.[8] By introducing the "magnetic pivot" concept,[10] these functions are modified to account for the fact that the mechanical pivot is not located in the plane of the gap magnetic surfaces.

The derivation of the permeance of gap B (P_b) will serve to illustrate the method. The region between the armature and pole B is divided into 11 simple geometric elements as shown in Fig. 18. Each element represents a region of flux paths. Total gap permeance is the sum of the individual permeances, each defined in terms of gap geometry as shown below:

$P_1(\theta)$ = permeance of main gap

$$P_1(\theta) = \begin{cases} \dfrac{\mu_o F_b}{\theta} \ln\left(\dfrac{\theta B_2 + L_{mg}}{\theta B_1 + L_{mg}}\right) \text{ for } \theta \neq 0 \\ \\ \mu_o F_b \left(\dfrac{B_2}{\theta B_2 + L_{mg}} - \dfrac{B_1}{\theta B_1 + L_{mg}}\right) \text{ for } |\theta| \ll \dfrac{L_{mg}}{B_1} \end{cases} \tag{22}$$

P_2 = permeance of one-half of a semicircular cylinder with length F_b and radius $\theta B_1 + L_{mg}$

$$P_2 = 0.52\ \mu_o F_b \tag{23}$$

$P_3(\theta)$ = permeance of a quarter annulus with axial length F_b and bounding radii of $\theta B_1 + L_{mg}$ and $\theta B_1 + L_{mg} + t$

$$P_3(\theta) = \frac{2\mu_o F_b}{\pi} \ln\left(1 + \frac{t}{\theta B_1 + L_{mg}}\right) \tag{24}$$

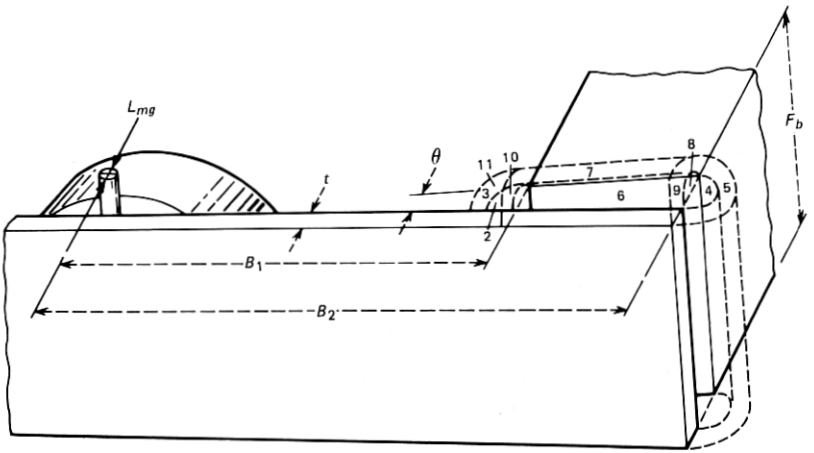

Fig. 18—Flux paths at gap B.

P_4 = permeance of a semicircular cylinder with length F_b and diameter $\theta B_2 + L_{mg}$

$$P_4 = 0.26\ \mu_o F_b \tag{25}$$

$P_5\ (\theta)$ = permeance of a half annulus with axial length F_b and bounding radii of $\frac{1}{2}(\theta B_2 + L_{mg})$ and $\frac{1}{2}(\theta B_2 + L_{mg}) + t$

$$P_5(\theta) = \frac{\mu_o F_b}{\pi} \ln\left(1 + \frac{2t}{\theta B_2 + L_{mg}}\right) \tag{26}$$

P_6 = permeance of a semicircular cylinder with length $B_2 - B_1$ and average diameter $\theta(B_2 + B_1)/2 + L_{mg}$

$$P_6 = 0.26\ \mu_o\ (B_2 - B_1) \tag{27}$$

$P_7\ (\theta)$ = permeance of a half annulus with length $B_2 - B_1$ and average bounding radii of

$$\frac{\theta}{2}\left(\frac{B_2 + B_1}{2}\right) + \frac{L_{mg}}{2}$$

and

$$\frac{\theta}{2}\left(\frac{B_2 + B_1}{2}\right) + \frac{L_{mg}}{2} + t$$

$$P_7(\theta) = \frac{\mu_o(B_2 - B_1)}{\pi} \ln\left(1 + \frac{2t}{\theta\left(\frac{B_2 + B_1}{2}\right) + L_{mg}}\right) \tag{28}$$

$P_8(\theta)$ = permeance of a spherical quadrant with diameter $\theta B_2 + L_{mg}$

$$P_8(\theta) = 0.077\ \mu_o(\theta B_2 + L_{mg}) \tag{29}$$

P_9 = permeance of a quadrant of a spherical shell with bounding radii of $\frac{1}{2}(\theta B_2 + L_{mg})$ and $\frac{1}{2}(\theta B_2 + L_{mg}) + t$

$$P_9 = \frac{\mu_o t}{4} \tag{30}$$

$P_{10}(\theta)$ = permeance of a spherical quadrant with diameter $\theta B_1 + L_{mg}$

$$P_{10}(\theta) = 0.077\ \mu_o(\theta B_1 + L_{mg}) \tag{31}$$

P_{11} = permeance of a quadrant of a spherical shell with bounding radii of $\frac{1}{2}(\theta B_1 + L_{mg})$ and $\frac{1}{2}(\theta B_1 + L_{mg}) + t$

$$P_{11} = \frac{\mu_o t}{4} \tag{32}$$

Now we can write $P_b(\theta)$, the total permeance of gap B:

$$P_b(\theta) = P_1(\theta) + P_2 + P_3(\theta) + P_4 + P_5(\theta) + 2P_6 + 2P_7(\theta) + 2P_8(\theta) + 2P_9 + 2P_{10}(\theta) + 2P_{11} \tag{33}$$

Since $P_2 = 2P_4$ and $P_9 = P_{11}$,

$$P_b(\theta) = P_1(\theta) + P_3(\theta) + 3P_4 + P_5(\theta) + 2P_6 + 2P_7(\theta) + 2P_8(\theta) + 2P_{10}(\theta) + 4P_{11} \tag{34}$$

The total permeance of gap B (34 and 22 to 32) has now been expressed in terms of ringer motor parameters. The permeance is then differentiated with respect to θ for use in the torque eq. (21). Gap A and the magnet-to-armature gap are handled in the same way.

APPENDIX E

Criterion function

The first term in the function to be minimized is the reciprocal of the torque factor squared. The rest of the terms are constraints imposed by means of penalty functions. Refer to Fig. 10 and the definitions in Section VII. Let

$R_1 = 1/(\text{torque factor})^2$

$R_2 = T_a$

$R_3 = T_b$

$R_4 = T_1$

$R_5 = T_3 - T_2$

R_6 = estimate of inductance

R_7 = thickness of shim in gap A

$$R_8 = \text{roll over} = \frac{(\text{torque factor from } I_2 \text{ to } I_3)}{(\text{torque factor from } I_1 \text{ to } I_2)}$$

Then let

$$D_i = 0, R_{\min_i} \leq R_i \leq R_{\max_i}$$

$$D_i = R_i - R_{\min_i}, R_i < R_{\min_i}$$

$$D_i = R_{\max_i} - R_i, R_i > R_{\max_i}$$

The criterion function P is formed by taking the weighted sum of the ${D_i}^2$.

$$P = \sum_{i=1}^{8} A_i {D_i}^2$$

The designer controls the optimization process by judicially choosing the weighting factors A_i and the constraints $R_{\min_i}$ and $R_{\max_i}$.

REFERENCES

1. A. H. Inglis and W. L. Tuffnell, "An Improved Telephone Set," B.S.T.J., *30,* No. 2 (April 1951), pp. 239–270.
2. Henry W. Ott, "Ringing Problems on Long Subscriber Loops," Telephony, *186,* No. 25 (June 24, 1974), pp. 33–40.
3. J. R. Power, "Flux Modulated Ringer," U.S. Patent 2,716,232, August 23, 1955.
4. W. Kalin and J. R. Power, "Audible Signal For Field Telephone Sets," U.S. Patent 2,658,194, November 3, 1953.
5. R. W. Kulterman and L. F. Mattson, "Computerized Analysis of Magnetically Coupled Electromechanical Systems," IEEE Transactions on Magnetics, *MAG-5,* No. 3 (September 1969).
6. U. Rauterberg, "Calculation and Optimization of Magnet Systems by Computer," 22nd Annual National Relay Conf. at Oklahoma State University, Stillwater, Oklahoma, April 30–May 1, 1974, paper No. 7 in Conf. Proc.
7. R. M.-M. Chen, C. F. Hempstead, Y. L. Kuo, M. L. Liou, R. P. Snicer, and E. D. Walsh, "Role of Computing and Precision Measurement," B.S.T.J., *53,* No. 10 (December 1974), pp. 2249–2253.
8. H. C. Roters, *Electromagnetic Devices,* first ed., New York: Wiley, 1941, Chap. 5.
9. J. Meisel, *Principles of Electromechanical-Energy Conversion,* New York, McGraw-Hill, 1966, Chap. 3.
10. M. S. Stein and B. S. Bengtsson, "The Working Air Gap of the EMR," paper presented at the 21st Annual National Relay Conf. at Oklahoma State University, Stillwater, Oklahoma, May 1–2, 1973, paper no. 16 in Conf. Proc.